ACS OMEGA

http://pubs.acs.org/journal/acsodf

Article

Long-Range Single-Molecule Förster Resonance Energy Transfer between Alexa Dyes in Zero-Mode Waveguides

Mikhail Baibakov, Satyajit Patra, Jean-Benoît Claude, and Jérôme Wenger*

Cite This: *ACS Omega* 2020, 5, 6947−6955

Read Online

ACCESS | Metrics & More | Article Recommendations

ABSTRACT: Zero-mode waveguide (ZMW) nano-apertures milled in metal films were proposed to improve the Förster resonance energy transfer (FRET) efficiency and enable single-molecule FRET detection beyond the 10 nm barrier, overcoming the restrictions of diffraction-limited detection in a homogeneous medium. However, the earlier ZMW demonstrations were limited to the Atto 550−Atto 647N fluorophore pair, asking the question whether the FRET enhancement observation was an artifact related to this specific set of fluorescent dyes. Here, we use Alexa Fluor 546 and Alexa Fluor 647 to investigate single-molecule FRET at large donor−acceptor separations exceeding 10 nm inside ZMWs. These Alexa fluorescent dyes feature a markedly different chemical structure, surface charge, and hydrophobicity as compared to their Atto counterparts. Our single molecule data on Alexa 546−Alexa 647 demonstrate enhanced FRET efficiencies at large separations exceeding 10 nm, extending the spatial range available for FRET and confirming the earlier conclusions. By showing that the FRET enhancement inside a ZMW does not depend on the set of fluorescent dyes, this report is an important step to establish the relevance of ZMWs to extend the sensitivity and detection range of FRET, while preserving its ability to work on regular fluorescent dye pairs.

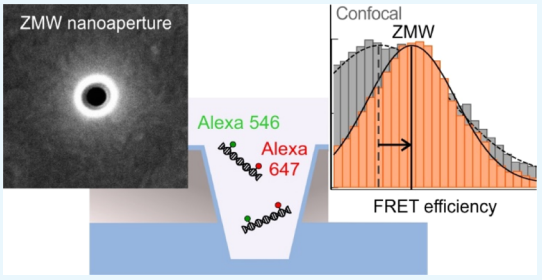

INTRODUCTION

Single-molecule Förster resonance energy transfer (smFRET) is a highly sensitive approach to investigate intra- and intermolecular distances on the nanometer scale,[1] revealing dynamics information about biomolecular structures and interactions.[2,3] However, the energy transfer efficiency quickly vanishes when the donor−acceptor separation grows, making smFRET measurements highly challenging at distances above 10 nm.[4,5] Extending smFRET to large biomolecular constructs requires the use of elaborated donor−acceptor constructs, and several strategies have been investigated using lanthanides,[6−8] quantum dots,[9,10] multicolor-cascaded systems,[11,12] gold nanoparticle quenchers,[13−15] metal-induced energy transfer,[16,17] or multiple fluorophores.[18−20] Because they do not rely on the organic fluorescent dye pairs conventionally used in smFRET such as Cy3−Cy5, for instance, these advanced approaches further complicate the sample preparation and data analysis. For many applications, it would be desirable to extend the smFRET range using regular fluorophore pairs.

Since the studies by Purcell and Drexhage,[21,22] it is established that the fluorescence emission decay rate is not only determined by the molecular structure but also depends on the photonic environment surrounding the molecule. The presence of a mirror (or a more elaborated optical component) can affect the fluorescence decay kinetics and the fluorescence lifetime. In a conceptually similar fashion, the dipole−dipole interaction leading to FRET can also be influenced by the photonic environment in some cases.[23−26] This opens a broad field of research using mirrors,[27−31] microcavities,[23,26,32,33] nano-apertures,[34−40] nanoparticles,[41−48] nanogap antennas,[49−53] or hyperbolic metamaterials.[54,55] Tuning FRET with nanophotonics can potentially overcome the 10 nm barrier in diffraction-limited confocal microscopes while still using conventional fluorophore pairs. However, reaching an enhancement of the FRET efficiency requires a delicate balance between the FRET rate and the other donor radiative and nonradiative processes,[47,48,51,55] while in many cases, the FRET efficiency can end up being quenched by the nanophotonic element.[27,33,48,50,51]

We have recently shown that nano-apertures milled in an opaque aluminum film [the so-called zero-mode waveguides (ZMWs)[56,57]] can improve the FRET efficiency and enable smFRET detection beyond the 10 nm barrier.[58] ZMWs are promising devices to perform smFRET on large biomolecular constructs with conventional dyes. However, the demonstration was so far limited to Atto 550−Atto 647N FRET pairs.[58] Both of these fluorescent molecules bear a positive charge after DNA labeling and have been found to be quite hydro-

Received: January 23, 2020
Accepted: March 5, 2020
Published: March 17, 2020

https://dx.doi.org/10.1021/acsomega.0c00322
ACS Omega 2020, 5, 6947−6955

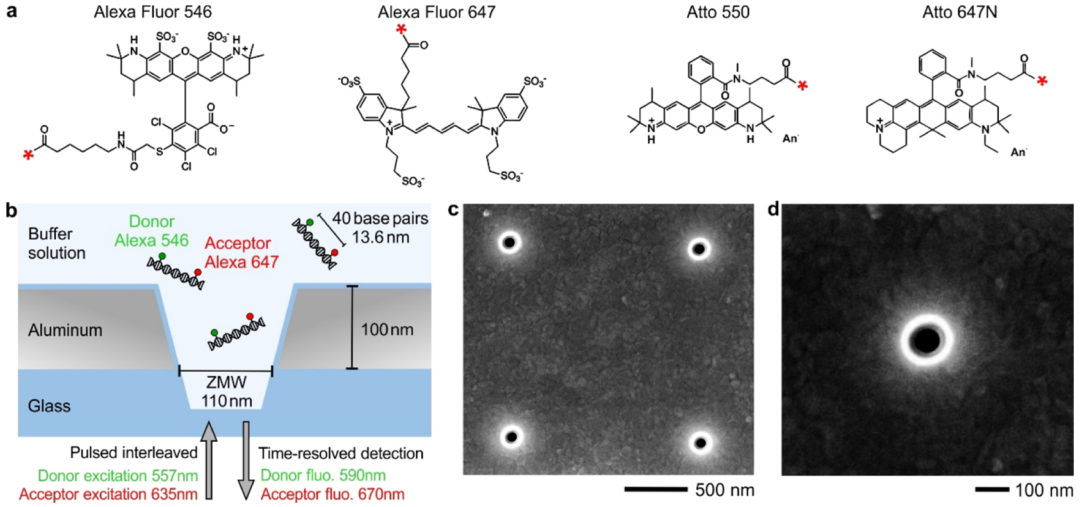

Figure 1. (a) Chemical structures of Alexa and Atto fluorescent molecules used as FRET pairs. The red star indicates the DNA-labeling site. (b) Experimental scheme of double-stranded DNA molecules containing a single Alexa Fluor 546 (donor) and Alexa Fluor 647 (acceptor) FRET pair. DNA is free to diffuse across the ZMW volume where it experiences pulsed interleaved excitation with alternating green and red laser pulses. (c,d) Scanning electron microscopy images of the pattern with ZMWs and a single ZMW of 110 nm diameter milled in an aluminum film.

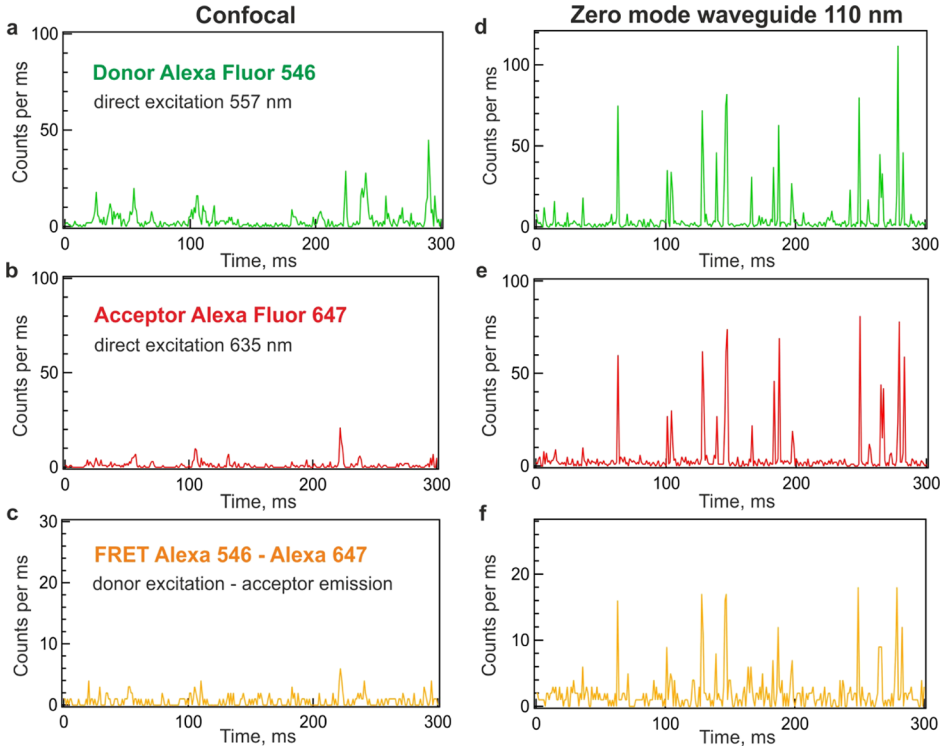

Figure 2. Fluorescent time traces of single Alexa 546−Alexa 647 FRET pairs with 13.6 nm (40 bp) separation diffusing in the confocal setup (a−c) and in a 110 nm-diameter ZMW (d−f) with a 0.5 ms binning time. The traces (a,d) show the donor emission after donor direct excitation at 557 nm, the traces (b,e) show the acceptor emission after acceptor direct excitation at 635 nm, and the traces (c,f) show the FRET emission (acceptor fluorescence) after donor excitation at 557 nm. The fluorescence enhancement in the ZMW directly leads to brighter detection events (d−f) as compared to the confocal reference (a−c) without any postprocessing.

phobic.[59,60] They also bear a higher affinity for glass or metal surfaces, which was observed for Atto 550 and Atto 647N dyes as compared to their cyanine or Alexa Fluor counterparts.[59−62] Although care was taken in our previous work to properly passivate the ZMW surface,[58,62] we cannot fully exclude that the observed enhanced FRET could be related to this specific choice of the FRET pair from Atto dyes.

Here, we build on the methodology previously developed for smFRET inside a ZMW[58] and explore the enhancement of smFRET efficiency for the Alexa Fluor 546−Alexa Fluor 647 donor−acceptor pair. This FRET pair, although spectrally quite similar to the Atto 550−Atto 647N pair, has a markedly different chemical structure and behavior (Figure 1a). Both Alexa 546 and Alexa 647 feature a negative charge once labeled to DNA, while Atto 550 and 647N dyes have a positive charge. It was observed that these Alexa dyes are more hydrophilic than their Atto counterparts[59,60] and that Atto 550 and 647N could induce surface adhesion of the DNA molecules while

https://dx.doi.org/10.1021/acsomega.0c00322
ACS Omega 2020, 5, 6947−6955

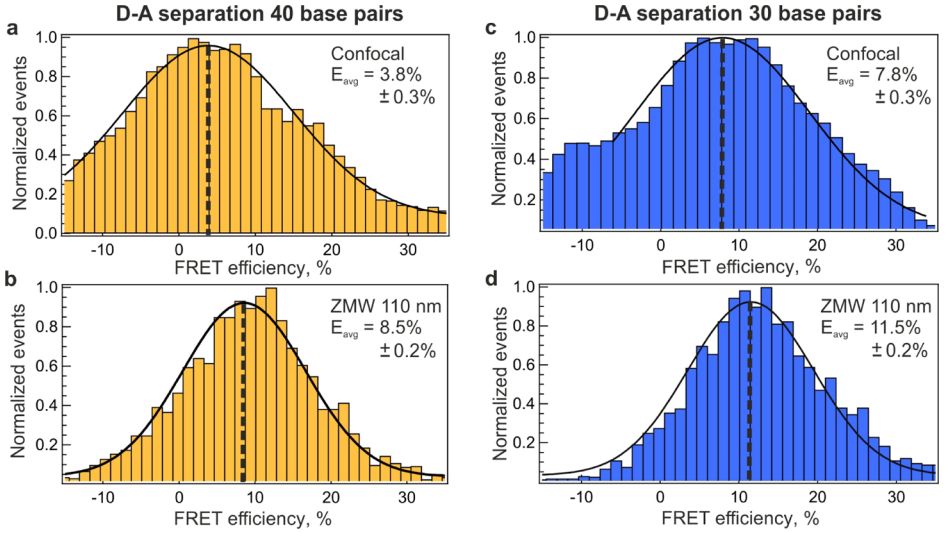

Figure 3. Enhancement of the FRET efficiency between Alexa Fluor dyes inside a ZMW. (a,c) smFRET efficiency histograms measured in a confocal configuration for Alexa 546−Alexa 647 FRET pairs with 40 and 30 bp, respectively (13.6 and 10.2 nm). (b,d) Same as (a,c) recorded in a ZMW of 110 nm diameter. Black lines are numerical fits with a Gaussian distribution to determine average FRET efficiency (thick dashed line). The average FRET efficiency is indicated for each plot, and the error bar corresponds to one standard deviation of the average value estimate.

Alexa 546 and 647 did not.[62] To assess the relevance of ZMWs for smFRET enhancement, it is thus necessary to quantify their performance for a clearly different set of dyes than the Atto 550−Atto 647N pair used so far.[35,36,50,58] Our new measurements for Alexa 546−Alexa 647 smFRET inside aluminum ZMWs demonstrate enhanced smFRET efficiencies at separations exceeding 10 nm, confirming the earlier conclusions drawn with Atto dyes. The detailed characterization reported here is an important step to establish the relevance and validity of ZMWs to extend the FRET detection range. As an additional advantage, all the smFRET measurements in the ZMWs are performed at 100 nM concentration, which is thousand-fold more concentrated than the conditions typically used for confocal detection. This brings smFRET analysis closer to physiological concentrations.[63,64]

RESULTS AND DISCUSSION

The FRET sample consists of double-stranded DNA molecules of 51 bp length, labeled with a single Alexa 546 donor and a single Alexa 647 acceptor. The donor−acceptor distance is fixed to 30 or 40 bp depending on the DNA construct (see the Methods section for the detailed DNA sequences and sample preparation). These fluorescent dyes feature a different surface charge and hydrophobicity as compared to Atto 550 and Atto 647N. Alexa 546 and Alexa 647 bear a negative charge after covalent linking to DNA, whereas Atto 550 and 647N have a positive charge (Figure 1a). A quantitative distinction between the hydrophobicity found for Alexa and Atto dyes can be done by comparing their distribution coefficient log D, with D denoting the ratio of the solute concentration in a nonpolar and polar solvent. Positive values of log D indicate hydrophobicity (Atto 550 and Atto 647N have log D values of 6.41 and 3.26, respectively), while negative values demonstrate hydrophilicity (Alexa 546 and Alexa 647 have log D values of −1.43 and −4.26, respectively).[60]

Our experiments monitor the FRET events stemming from individual molecules diffusing across the detection volume (Figure 1b). To clearly quantify the FRET efficiency and avoid the issues related to incomplete fluorophore labeling, we implement pulsed interleaved excitation (PIE) using two alternating laser excitations to excite the donor and acceptor dyes in a sequential manner.[65,66] PIE allows to postselect the events corresponding to an active FRET pair, where both dyes are fluorescent, and discard all the cases where only the donor is present.

The main difference as compared to a conventional diffraction-limited microscope is the use of ZMW nanoapertures to confine the light into attoliter volumes.[56,57] The ZMWs used here are milled in a 100 nm-thick aluminum film with a diameter of 110 nm (Figure 1c,d). Although the use of Atto 550−Atto 647N dyes requires the ZMW to be passivated with a silane-modified polyethylene glycol in order to avoid surface adsorption of the DNA molecules,[62] for Alexa 546−Alexa 647, we find that similar results can be obtained with and without the surface passivation step. This additional advantage of the Alexa FRET pair further simplifies the experimental preparation.

Figure 2 shows typical fluorescence time traces recorded with the confocal setup and with a 110 nm-diameter ZMW. In order to ensure that the fluorescence bursts correspond to single molecules passing through the observation volume and to have a negligible probability to observe more than one molecule, we use a low concentration of the DNA sample: 100 pM for confocal and 100 nM for ZMWs. Brighter detection events are directly obtained with the ZMW (Figure 2d−f) as compared to the confocal reference (Figure 2a−c), which illustrates one specific advantage of the fluorescence enhancement occurring inside ZMWs as an improvement for the net detected fluorescence brightness.[67] We analyze the total fluorescence time trace using fluorescence correlation spectroscopy (FCS) to compute the temporal autocorrelation and estimate the average number of emitters and their average brightness. Following our previous studies,[58,67] this quantifies the fluorescence brightness enhancement factor for isolated donor and acceptor molecules. For Alexa 546, we find a gain of 11.4 ± 0.9 in a 110 nm ZMW, while for Alexa 647, the enhancement is 15.9 ± 1.2. The fact that a higher enhancement is observed for the red dye is mostly related to

https://dx.doi.org/10.1021/acsomega.0c00322
ACS Omega 2020, 5, 6947−6955

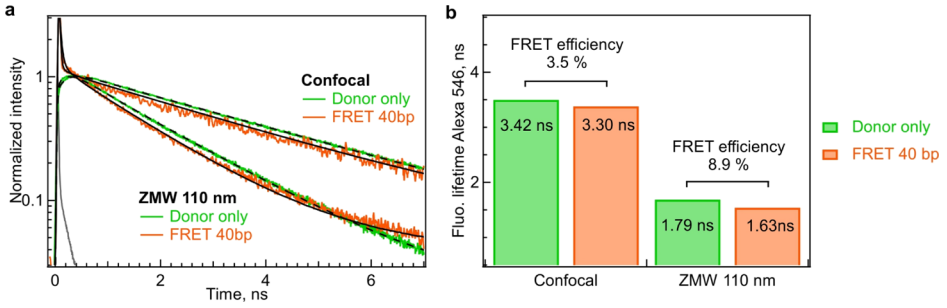

Figure 4. (a) Normalized donor fluorescence lifetime decay traces in confocal and in a 110 nm-diameter ZMW. Black lines are fits for lifetime traces. For both ZMW and confocal cases, the presence of the acceptor (FRET case) further accelerates the donor decay dynamics, which is a clear signature for FRET. All fit details are summarized in Table 1 and in the Methods section. (b) Intensity-averaged fluorescence lifetimes deduced from the traces in (a), which allow an independent measurement of the average FRET efficiency based on the Alexa 546 donor lifetime reduction.

the lower quantum yield of the dye (33% for Alexa 647 and 79% for Alexa 546), as low quantum yield emitters lead to the observation of higher enhancement factors.[68]

Using these fluorescence time traces (the total length is 120 s and accumulates over 2000 detection events), we apply the standardized smFRET analysis protocol detailed in ref 1 (see Methods for details). After the PIE postselection, we compute the FRET efficiency (E_{FRET}) for each burst, taking into account the donor crosstalk, the acceptor direct excitation, and the different quantum yields and detection efficiencies between the dyes. The influence of the ZMW is fully taken into account by calibrating the correction parameters for each ZMW independently. The aluminum ZMWs used here are optically weakly resonant components, which do not noticeably modify the fluorescence spectrum of the dyes. Therefore, as we detail in the Methods section, most correction parameters (for crosstalk and direct excitation) are unchanged in the ZMW as compared to the confocal case.

Figure 3a,b compares the smFRET efficiency histograms for the Alexa 546−Alexa 647 construct with 40 bp separation (corresponding to an average D−A distance of about R = 13.6 nm) for the confocal setup and the ZMW. For this D−A separation, which is about twice the R_0 = 7.4 nm Förster radius for this FRET pair, the average FRET efficiency in the confocal case is only 3.8 ± 0.3%. To estimate the uncertainty $\sigma_{average}$ on the average FRET efficiency, we apply the classical formula $\sigma_{average} = \sigma/\sqrt{N}$, where σ is the standard deviation of the Gaussian distribution fit and N is the total number of detected bursts (typically 2000). Using the Förster formula $1/(1 + (R/R_0)^6)$ gives a 2.5% estimate for the average FRET efficiency in the confocal case for the 40 bp separation. However, this approach is limited by the uncertainties on both R and R_0 and the assumption of perfectly random orientation for both dyes, which may not be fully verified by our real sample. Thanks to the optical confinement occurring in the ZMW, the FRET efficiency is improved up to 8.5 ± 0.2% inside the 110 nm ZMW. Moreover, the full statistical distributions are clearly different, and smFRET is better detected in the ZMW case thanks to higher average FRET efficiencies and narrower distributions. In the confocal case, the standard deviation of the Gaussian distribution (Figure 3a,c) is 12%, while it is reduced inside the ZMW to 8% thanks to the higher fluorescence brightness.

We also investigate shorter separations of 30 bp (D−A distance ≈ 10.2 nm). As the acceptor is brought closer to the donor, the average FRET efficiency is increased to 7.8 ± 0.3% in the confocal setup (Figure 3c) and is further enhanced to 11.5 ± 0.2% in the ZMW (Figure 3d). Computing the gains in the average FRET efficiencies brought by the ZMW, we find a gain of 2.2× (±0.2) for the 40 bp separation and 1.5× (±0.1) for the 30 bp case. First, these values demonstrate that the ZMW can indeed improve the net detected FRET efficiency for Alexa FRET pairs, which is especially relevant at large D−A separations exceeding 10 nm where confocal microscopes face their limit of detection. It was observed previously with nanoapertures,[35] nanoantennas,[50] and planar microcavities[26] that the enhancement factors for the FRET rate were higher for the samples corresponding to the larger D−A separations. In other words, the influence of the nanophotonic structure is more pronounced when the D−A separation is larger. We retrieve this feature here. The main reason behind this is that the nanophotonic structure influence on the FRET rate is quite weak as compared to that on the FRET rate between two closely separated fluorescent dyes in a homogeneous environment. Therefore, one has to go to D−A distances greater than 10 nm so that the ZMW relative influence becomes more prominent.[58] Second, we can compare the results for Alexa and Atto FRET pairs. For Atto 550−Atto 647N, our previous measurements indicated a gain of 2.9× (±0.3) for the 40 bp separation and 1.2× (±0.1) for the 30 bp case,[58] which are quite comparable to the results found here with Alexa dyes despite their different chemical structures. This suggests that the smFRET enhancement inside ZMWs does not depend on the type of fluorescent dyes used.

Independent of the FRET analysis in Figure 3, the average FRET efficiency can also be assessed from the reduction of the donor lifetime because of the presence of the acceptor, using the formula $E_{FRET} = 1 - \tau_{DA}/\tau_D$, where τ_{DA} and τ_D are the fluorescence lifetimes of the donor in the presence and absence of acceptor, respectively.[2] This approach importantly provides an independent control on the estimated FRET efficiencies and does not require any separate calibration to account for donor crosstalk, acceptor direct excitation, or quantum yield difference. Figure 4a shows the normalized fluorescence decay traces for the Alexa 546 donor in the confocal setup and in a 110 nm-diameter ZMW, both with and without an Alexa 647 acceptor. Without any data processing, it is apparent on the fluorescence decays that the presence of the acceptor dye accelerates the donor decay dynamics. This provides a direct evidence for the occurrence of FRET and not of radiative energy transfer mediated by a propagating photon. The donor lifetime change due to the acceptor occurs only in FRET where the dipoles are coupled in the near field via evanescent waves. On the contrary, the donor lifetime is unchanged when the

https://dx.doi.org/10.1021/acsomega.0c00322
ACS Omega 2020, 5, 6947−6955

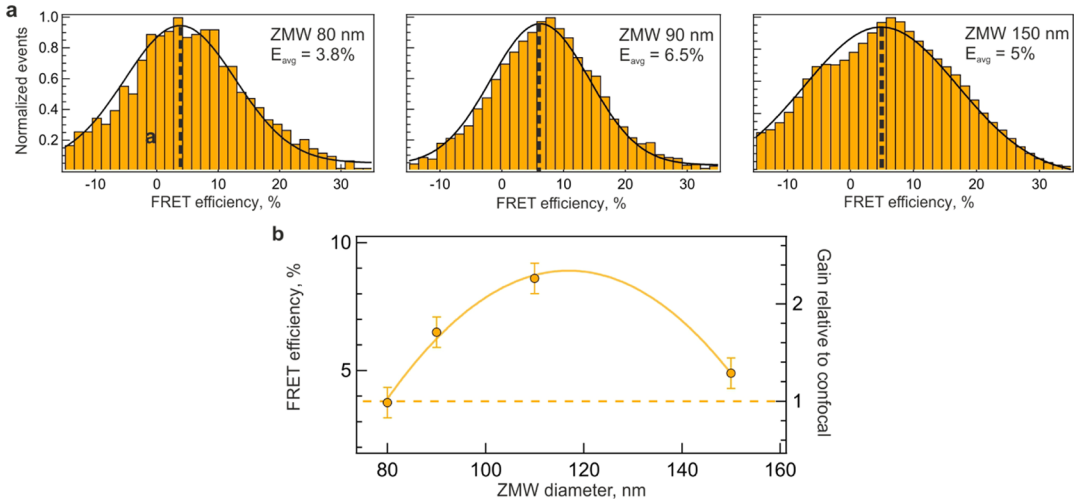

Figure 5. (a) smFRET efficiency histograms with ZMWs of different diameters. The DNA sample consists of Alexa 546 donor−Alexa 647 acceptor with 40 bp separation similar to Figure 3b. (b) FRET efficiency (left axis) and FRET efficiency gain (right axis) as a function of the ZMW diameter for Alexa 546−Alexa 647 with 40 bp separation. The horizontal dashed line indicates the level found for the confocal reference. The error bar on the graph corresponds to two times the standard deviation on the mean FRET efficiency estimate.

dipoles are coupled through radiative transfer, where the energy travels in the form of a propagating photon and can be funneled by the presence of a waveguide.[69−72] The analysis of the traces in Figure 4a quantifies the τ_D and τ_{DA} lifetimes used to compute the average FRET efficiency (Figure 4b, see details in the Methods section). An excellent agreement is found with the results derived from the smFRET histograms in Figure 3a,b, with a difference of less than 0.4% for both the confocal setup and the ZMW. This further confirms the validity of our results.

Although the various results demonstrate the FRET enhancement inside a ZMW of 110 nm diameter, we now investigate the influence of the ZMW diameter on the energy transfer between Alexa dyes. The same procedure as for Figure 3 is applied for ZMW diameters ranging from 80 to 150 nm (Figure 5a). A gradual shift of the mean FRET efficiency is observed in the distributions, which is summarized as a function of the ZMW diameter in Figure 5b. Here, the 110 nm diameter used, as shown in Figure 3, is near optimum. Using a large diameter, the fluorescence enhancement decreases and the FRET results tend to retrieve the confocal values. Using a lower diameter, the quenching losses due to direct energy transfer to the metal increase, which compete with FRET to the acceptor dye and reduce the observed FRET efficiency.

CONCLUSIONS

Our data demonstrate here that the phenomenon of smFRET enhancement inside a ZMW is quite general and does not depend on the type of fluorescent dyes used. Performing smFRET measurements on Alexa 546−Alexa 647 pairs, which feature a markedly different chemical structure, surface charge, and hydrophobicity, as compared to their Atto 550−Atto 647N counterparts, we retrieve the same conclusions about the quantitative performance of ZMWs to enhance smFRET. Notably, we could achieve over a twofold enhancement of the net detected FRET efficiency for dyes separated by more than 10 nm. This significantly improves the sensitivity and detection range of smFRET, while preserving the ability to work on conventional fluorophore pairs. The only difference as compared to a classical confocal microscope concerns the replacement of the glass coverslip by a coverslip holding ZMW nano-apertures, which are easy to fabricate using various lithography techniques. The ZMW confine the detection volume to the attoliter range, enabling single-molecule FRET detection at a 100 nM concentration. This 1000-fold higher concentration for smFRET than with a diffraction-limited confocal microscope is especially interesting for exploring protein−protein and protein−DNA interactions, featuring lower affinities.[63,64] It should be reminded that the Förster formula $1/(1 + (R/R_0)^6)$ is only valid for a homogeneous medium and can no longer be applied directly in the vicinity of a nanophotonic structure. Inside a ZMW, both the R_0 and the $1/R^6$ decay are affected. Although the changes remain minimal for distances below 8−10 nm,[35,36] some significant deviations can be found for D−A distances greater than 10 nm, where the FRET enhancement becomes important, as demonstrated in this work. Therefore, preliminary calibrations should be performed in order to enable relevant distance measurements using FRET in ZMWs (and this work contributes to it), but conceptually, there is no reason why quantitative distance measurements would not be possible using FRET inside ZMWs.

METHODS

ZMW Fabrication. A 100 nm thick layer of aluminum is deposited on a clean glass coverslip by electron-beam evaporation (Bühler Syrus Pro 710).[58] The deposition rate is 10 nm/s at a chamber pressure of 5×10^{-7} mbar.[73] Individual ZMWs are then milled with a gallium-based focused ion beam (FEI dual beam DB 235 Strata) set at 10 pA current and 30 kV voltage. The gallium ion beam has a resolution of about 10 nm. ZMWs are cleaned using UV−ozone during 5 min and rinsed with water and ethanol to remove any organic impurities before the measurements.

Alexa Dye FRET Samples. The FRET sample consists of double-stranded DNA with the forward strand being labeled with Alexa Fluor 546 (donor) and its complementary strand being labeled with Alexa Fluor 647 (acceptor). The DNA strands are obtained from IBA life solution (Göttingen, Germany) and are HPLC-purified. The forward strand

https://dx.doi.org/10.1021/acsomega.0c00322
ACS Omega 2020, 5, 6947−6955

sequence of the DNA is 5′-CCT GAG CGT ACT GCA GGA TAG CCT ATC GCG TGT CAT ATG CTG TTC AGT GCG-3′ where the thymine at position 44 is labeled with Alexa Fluor 546. The complementary reverse strand is 5′-CGC ACT GAA CAG CAT ATG ACA CGC GAT AGG CTA TCC TGC AGT ACG CTC AGG-3′ where the T base at position 47 is labeled with Alexa Fluor 647. In this configuration, we get a 40 bp separation between donor and acceptor dyes corresponding to approximately 13.6 nm. For the sample with 10.2 D−A separation (30 bp), the T base at position 37 is instead labeled with Alexa Fluor 647. The forward and reverse strands are hybridized in a buffer containing 5 mM Tris, 20 mM $MgCl_2$, and 5 mM NaCl at pH 7.5. First, the mixture is heated at 90 °C for 5 min. Then, the mixture is cooled down to room temperature for 3 h. The concentration of 100 pM and 100 nM is used for the smFRET measurements in confocal microscopy and in ZMWs, respectively, in a buffer containing 20 mM Hepes, 10 mM NaCl, and 0.1% Tween 20 at pH 7.5.

Experimental Setup. The confocal microscope setup has been detailed in ref 58. Briefly, the Alexa 546 donor is excited at 557 nm using an iChrome-TVIS laser (Toptica), and the Alexa 647 acceptor is excited at 635 nm using an LDH laser diode (PicoQuant). Green and red pulses are alternating at a 40 MHz repetition rate in a PIE configuration,[66,74] with 20 μW average power low enough to avoid fluorescence saturation or photobleaching on the diffusing dyes. Both lasers have linear polarizations which are set parallel to each other. No polarization selection is performed on the fluorescence detection. The microscope objective is a Zeiss C-Apochromat 63× with a 1.2 NA water immersion objective used in an epifluorescence configuration. For detecting donor and acceptor fluorescence, two MPD-5CTC avalanche photodiodes (PicoQuant) are employed together with 50 μm confocal pinholes and spectral filters (donor fluorescence collection from 570 to 620 nm, acceptor fluorescence collection from 655 to 750 nm). The photodiode signals are connected to a HydraHarp 400 single photon counting module (PicoQuant) in a time-tagged time-resolved mode. The overall system timing resolution is 38 ps (full width at half-maximum).

FRET Efficiency Measurements. The procedure to compute the FRET efficiency histograms follows the standard approach in smFRET.[1,74] First, we select the single-molecule detection events and separate them from the background noise, applying a threshold criterion so that the sum of the signals in donor and acceptor channels exceeds 25 counts per ms for the ZMW (12 counts per ms for the confocal case). A second threshold is used to check the presence of the red dye upon the excitation using the red laser. We choose the value at 12 counts per ms in the acceptor channel with red excitation (3 counts per ms for the confocal case because of the lower fluorescence brightness). We ensure that these levels have a negligible influence on the measured average FRET efficiencies.

The FRET efficiency is then calculated as[1,58]

$$E_{\mathrm{FRET}} = \frac{n_{\mathrm{A}}^{\mathrm{green}} - \alpha n_{\mathrm{D}}^{\mathrm{green}} - \delta n_{\mathrm{A}}^{\mathrm{red}}}{(n_{\mathrm{A}}^{\mathrm{green}} - \alpha n_{\mathrm{D}}^{\mathrm{green}} - \delta n_{\mathrm{A}}^{\mathrm{red}}) + \gamma n_{\mathrm{D}}^{\mathrm{green}}} \quad (1)$$

where $n_{\mathrm{D}}^{\mathrm{green}}$ and $n_{\mathrm{A}}^{\mathrm{green}}$ are the number of photons per each burst for the donor and acceptor channel upon excitation using a green laser, respectively, $n_{\mathrm{A}}^{\mathrm{red}}$ is the number of photons in the red channel with the excitation using the red laser. The numbers of photons are corrected for the background contribution in each channel. The background counts are measured by performing a separate experiment using the buffer solution only for the ZMW or the reference glass coverslip. The equation above contains correction factors for (1) the crosstalk α fraction of the donor emission collected in the acceptor detection channel, (2) the direct excitation δ of the acceptor by the green laser, and (3) the correction parameter γ which accounts for the difference of the quantum yields of the dyes (ϕ_{D}, ϕ_{A}) and their detection efficiencies between channels (κ_{d}, κ_{a}).

The crosstalk α is the ratio between the donor emission leaking into the acceptor channel as compared to the donor emission in the donor channel. The crosstalk is determined for the DNA sample containing only the donor fluorophore: $\alpha = \frac{n_{\mathrm{A}}^{\mathrm{green}}}{n_{\mathrm{D}}^{\mathrm{green}}}$. For all ZMW diameters, the crosstalk remains nearly constant $\alpha = 0.05$ with slight variation for 100 and 150 nm at $\alpha = 0.04$. We found a similar value for the confocal setup $\alpha = 0.05$.

The direct excitation δ corresponds to the fraction of the acceptor fluorescence because of direct excitation by the green laser as compared to the acceptor emission signal by the red laser. This parameter is measured when a DNA sample containing only the acceptor dye is excited: $\delta = \frac{n_{\mathrm{A}}^{\mathrm{green}}}{n_{\mathrm{A}}^{\mathrm{red}}}$. For the confocal reference, we find $\delta = 0.11$, which also does not change for ZMW diameters except for the 80 nm ZMW where we have $\delta = 0.08$.

The γ correction factor takes into account the differences in the fluorescence quantum yields (ϕ_{D}, ϕ_{A}) and the detection efficiencies (κ_{d}, κ_{a}): $\gamma = \frac{\kappa_{\mathrm{A}}\phi_{\mathrm{A}}}{\kappa_{\mathrm{D}}\phi_{\mathrm{D}}}$. For the Alexa 546−Alexa 647 FRET pair in our confocal setup, we compute $\gamma_{\mathrm{conf}} = 0.43 \pm 0.02$ from the knowledge of the fluorescence spectrum and quantum yield of each dye. The photodiode response is also accounted for in the calculation. Alternatively, the γ correction factor can also be estimated from the measured stoichiometry S[1] and the average fluorescence brightness per molecule $\mathrm{CRM}_{\mathrm{A}}^{\mathrm{red}}$ and $\mathrm{CRM}_{\mathrm{DO}}^{\mathrm{green}}$ measured by FCS following the approach used in ref 58

$$\gamma_{\mathrm{conf}} = \frac{S}{1 - S}\frac{\mathrm{CRM}_{\mathrm{A}}^{\mathrm{red}}}{\mathrm{CRM}_{\mathrm{DO}}^{\mathrm{green}}} \quad (2)$$

where $\mathrm{CRM}_{\mathrm{A}}^{\mathrm{red}}$ is for red excitation of the acceptor dye and $\mathrm{CRM}_{\mathrm{DO}}^{\mathrm{green}}$ is for green excitation of the sample containing only the donor dye. Using the measured values of $\mathrm{CRM}_{\mathrm{A}}^{\mathrm{red}} = 5000$ counts/s for Alexa 647 DNA, $\mathrm{CRM}_{\mathrm{DO}}^{\mathrm{green}} = 11{,}000$ counts/s for Alexa 546 DNA, and $S = 0.46$, we find $\gamma_{\mathrm{conf}} = 0.39 \pm 0.05$, in good agreement with the 0.43 ± 0.02 calculated value.

For the ZMW, γ is modified because of the different enhancement factors of the donor and acceptor and is found as[35,50,58]

$$\gamma_{\mathrm{ZMW}} = \gamma_{\mathrm{conf}} \times \frac{\mathrm{EnhCRM}_{\mathrm{AO}}^{\mathrm{green}}}{\mathrm{EnhCRM}_{\mathrm{DO}}^{\mathrm{green}}} = \gamma_{\mathrm{conf}} \times \frac{\delta_{\mathrm{ZMW}}}{\delta_{\mathrm{conf}}} \times \frac{\mathrm{EnhCRM}_{\mathrm{AO}}^{\mathrm{red}}}{\mathrm{EnhCRM}_{\mathrm{AO}}^{\mathrm{green}}} \quad (3)$$

where $\mathrm{EnhCRM}_{\mathrm{AO}}^{\mathrm{green}}$ and $\mathrm{EnhCRM}_{\mathrm{DO}}^{\mathrm{green}}$ are the fluorescence enhancement factors of the fluorescence count rate per molecule for acceptor-only and donor-only samples upon a green excitation, respectively, and $\mathrm{EnhCRM}_{\mathrm{AO}}^{\mathrm{red}}$ is for red

https://dx.doi.org/10.1021/acsomega.0c00322
ACS Omega 2020, 5, 6947−6955

excitation. All the enhancement factors are assessed by FCS for each ZMW diameter.[67] We find γ_{ZMW} for 80, 90, 110, and 150 nm to be 0.45, 0.65, 0.6, and 0.65, respectively. Except for the 80 nm ZMW (for which a significant fluorescence quenching is found), the γ correction factor does not vary much for ZMW diameters from 90 to 150 nm. In contrast to the case of the Atto 550−Atto 647N FRET pair,[58] for Alexa 546−Alexa 647, we find an increase in the γ correction factor in the ZMW as compared to the confocal reference ($\gamma_{ZMW} \approx 0.65$, while $\gamma_{conf} = 0.43$). According to eq 1, a higher γ value will lead to a decrease in the FRET efficiency (by increasing the denominator in the fraction). The net FRET efficiency enhancement observed inside the ZMW (Figures 3 and 5) shows that the gain in the acceptor emission n_A^{green} is enough to compensate for the increased γ factor.

Fluorescence Lifetime Analysis. In addition to the fluorescence burst analysis in eq 1, the average FRET efficiency can be independently determined from the donor fluorescence lifetime data. We use the equation $E_{FRET} = 1 - \tau_{DA}/\tau_D$, where τ_{DA} and τ_D are the fluorescence lifetimes of the donor in the presence and absence of the acceptor, respectively. To determine τ_{DA} and τ_D, we fit the time-correlated single photon counting (TCSPC) histograms (Figure 4a) with a reconvolution, taking into account the instrument response function (IRF), whose full width at half-maximum was measured to be 38 ps. All the lifetime analysis is performed using the SymPhoTime 64 software (PicoQuant). For the FRET data in Figure 4a, we use the same traces as for the intensity burst analysis in Figures 2 and 3, leading to an average number of molecules in the detection volume around 0.1 (concentrations of 100 pM and 100 nM for the confocal and ZMW cases). For the donor-only TCSPC data, we use 10 times higher concentrations (average number of detected molecules about 1) to achieve a better signal-to-noise ratio. As a consequence of the higher background contribution in the FRET cases, a peak at $t = 0$ is seen for the FRET TCSPC data. This peak corresponds to a sum of laser light scattering, metal photoluminescence, and Raman scattering. This contribution is interpolated with a fixed 20 ps component (shorter than the 38 ps IRF resolution) to achieve a complete fitting of the TCSPC decay, but this contribution is then discarded for the lifetime analysis as it only corresponds to noise. The background and scattering contributions are recorded by performing a separate experiment in the same conditions using only the buffer in the absence of the DNA sample. For the TCSPC analysis, we ensure that more than 92% of the total detected photons are considered for the fits. The data for the confocal reference (FRET and donor only) are fitted with a single exponential decay (excluding the fixed 20 ps contribution from laser scattering). For the ZMWs, a biexponential function with fast and slow components provides a better fit with flat residuals. As observed previously for Atto dyes,[58] the fast component converges toward values around 400 ps for both the FRET and donor-only samples inside a 110 nm ZMW. All the fit parameters are summarized in Table 1. The tail seen for long delay times higher than 5 ns is only due to the background level, and there is no supplementary long lifetime. In the ZMW case, the intensity-averaged lifetimes are used to compute the average FRET efficiency. We find empirically that these values provide a better match with the separate burst intensity analysis (Figure 3) than the amplitude-averaged data. However, our claim of enhanced FRET efficiency in the ZMW is maintained for all the approaches (intensity-averaged, amplitude-averaged, or direct comparison between long lifetime components).

Table 1. Results Obtained from the Numerical Fit to the TSCPC Histograms Shown in Figure 4a[a]

condition	sample	τ_1/ns	τ_2/ns	α_1	α_2	τ_{int}/ns	τ_{amp}/ns
confocal	D only	3.42		1		**3.42**	3.42
	D−A 40 bp	3.30		1		**3.30**	3.30
ZMW 110 nm	D only	1.89	0.40	0.76	0.24	**1.79**	1.54
	D−A 40 bp	1.77	0.40	0.67	0.33	**1.63**	1.32

[a]In the case of a biexponential fit, τ_1 and τ_2 are the individual lifetimes of each component and α_1 and α_2 are their respective normalized amplitudes. $\tau_{amp} = (\alpha_1\tau_1 + \alpha_2\tau_2)/(\alpha_1 + \alpha_2)$ is the amplitude-averaged lifetime, while $\tau_{int} = (\alpha_1\tau_1^2 + \alpha_2\tau_2^2)/(\alpha_1\tau_1 + \alpha_2\tau_2)$ denotes the intensity-averaged lifetime. The 20 ps scattering peak at $t = 0$ is not shown here.

AUTHOR INFORMATION

Corresponding Author

Jérôme Wenger − *Aix Marseille Univ, CNRS, Centrale Marseille, Institut Fresnel 13013 Marseille, France;* orcid.org/0000-0002-2145-5341; Email: jerome.wenger@fresnel.fr

Authors

Mikhail Baibakov − *Aix Marseille Univ, CNRS, Centrale Marseille, Institut Fresnel 13013 Marseille, France*

Satyajit Patra − *Aix Marseille Univ, CNRS, Centrale Marseille, Institut Fresnel 13013 Marseille, France;* orcid.org/0000-0002-1118-3741

Jean-Benoît Claude − *Aix Marseille Univ, CNRS, Centrale Marseille, Institut Fresnel 13013 Marseille, France*

Complete contact information is available at: https://pubs.acs.org/10.1021/acsomega.0c00322

Notes

The authors declare no competing financial interest.

ACKNOWLEDGMENTS

The authors thank Antonin Moreau and Julien Lumeau for help with the aluminum layer preparation. This project has received funding from the Agence Nationale de la Recherche (ANR) under grant agreement ANR-17-CE09-0026-01 and from the European Research Council (ERC) under the European Union's Horizon 2020 research and innovation programme (grant agreement no. 723241).

REFERENCES

(1) Hellenkamp, B.; Schmid, S.; Doroshenko, O.; Opanasyuk, O.; Kühnemuth, R.; Rezaei Adariani, S.; Ambrose, B.; Aznauryan, M.; Barth, A.; Birkedal, V.; Bowen, M. E.; Chen, H.; Cordes, T.; Eilert, T.; Fijen, C.; Gebhardt, C.; Götz, M.; Gouridis, G.; Gratton, E.; Ha, T.; et al. Precision and Accuracy of Single-Molecule FRET Measurements—a Multi-Laboratory Benchmark Study. *Nat. Methods* **2018**, *15*, 669−676.

(2) Lerner, E.; Cordes, T.; Ingargiola, A.; Alhadid, Y.; Chung, S.; Michalet, X.; Weiss, S. Toward Dynamic Structural Biology: Two Decades of Single-Molecule Förster Resonance Energy Transfer. *Science* **2018**, *359*, No. eaan1133.

(3) Roy, R.; Hohng, S.; Ha, T. A Practical Guide to Single-Molecule FRET. *Nat. Methods* **2008**, *5*, 507−516.

https://dx.doi.org/10.1021/acsomega.0c00322
ACS Omega 2020, 5, 6947−6955

(4) Schuler, B.; Hofmann, H. Single-Molecule Spectroscopy of Protein Folding Dynamics—Expanding Scope and Timescales. *Curr. Opin. Struct. Biol.* **2013**, *23*, 36−47.
(5) Hevekerl, H.; Spielmann, T.; Chmyrov, A.; Widengren, J. Förster Resonance Energy Transfer beyond 10 Nm: Exploiting the Triplet State Kinetics of Organic Fluorophores. *J. Phys. Chem. B* **2011**, *115*, 13360−13370.
(6) Selvin, P. R. Principles and Biophysical Applications of Lanthanide-Based Probes. *Annu. Rev. Biophys. Biomol. Struct.* **2002**, *31*, 275−302.
(7) Selvin, P. R.; Hearst, J. E. Luminescence Energy Transfer Using a Terbium Chelate: Improvements on Fluorescence Energy Transfer. *Proc. Natl. Acad. Sci. U.S.A.* **1994**, *91*, 10024−10028.
(8) Hildebrandt, N.; Wegner, K. D.; Algar, W. R. Luminescent Terbium Complexes: Superior Förster Resonance Energy Transfer Donors for Flexible and Sensitive Multiplexed Biosensing. *Coord. Chem. Rev.* **2014**, *273*−*274*, 125−138.
(9) Hildebrandt, N.; Spillmann, C. M.; Algar, W. R.; Pons, T.; Stewart, M. H.; Oh, E.; Susumu, K.; Díaz, S. A.; Delehanty, J. B.; Medintz, I. L. Energy Transfer with Semiconductor Quantum Dot Bioconjugates: A Versatile Platform for Biosensing, Energy Harvesting, and Other Developing Applications. *Chem. Rev.* **2017**, *117*, 536−711.
(10) Guo, J.; Qiu, X.; Mingoes, C.; Deschamps, J. R.; Susumu, K.; Medintz, I. L.; Hildebrandt, N. Conformational Details of Quantum Dot-DNA Resolved by Förster Resonance Energy Transfer Lifetime Nanoruler. *ACS Nano* **2019**, *13*, 505−514.
(11) Lee, N. K.; Kapanidis, A. N.; Koh, H. R.; Korlann, Y.; Ho, S. O.; Kim, Y.; Gassman, N.; Kim, S. K.; Weiss, S. Three-Color Alternating-Laser Excitation of Single Molecules: Monitoring Multiple Interactions and Distances. *Biophys. J.* **2007**, *92*, 303−312.
(12) Stein, I. H.; Steinhauer, C.; Tinnefeld, P. Single-Molecule Four-Color FRET Visualizes Energy-Transfer Paths on DNA Origami. *J. Am. Chem. Soc.* **2011**, *133*, 4193−4195.
(13) Yun, C. S.; Javier, A.; Jennings, T.; Fisher, M.; Hira, S.; Peterson, S.; Hopkins, B.; Reich, N. O.; Strouse, G. F. Nanometal Surface Energy Transfer in Optical Rulers, Breaking the FRET Barrier. *J. Am. Chem. Soc.* **2005**, *127*, 3115−3119.
(14) Riskowski, R. A.; Armstrong, R. E.; Greenbaum, N. L.; Strouse, G. F. Triangulating Nucleic Acid Conformations Using Multicolor Surface Energy Transfer. *ACS Nano* **2016**, *10*, 1926−1938.
(15) Samanta, A.; Zhou, Y.; Zou, S.; Yan, H.; Liu, Y. Fluorescence Quenching of Quantum Dots by Gold Nanoparticles: A Potential Long Range Spectroscopic Ruler. *Nano Lett.* **2014**, *14*, 5052−5057.
(16) Chizhik, A. I.; Rother, J.; Gregor, I.; Janshoff, A.; Enderlein, J. Metal-Induced Energy Transfer for Live Cell Nanoscopy. *Nat. Photonics* **2014**, *8*, 124−127.
(17) Ghosh, A.; Sharma, A.; Chizhik, A. I.; Isbaner, S.; Ruhlandt, D.; Tsukanov, R.; Gregor, I.; Karedla, N.; Enderlein, J. Graphene-Based Metal-Induced Energy Transfer for Sub-Nanometre Optical Localization. *Nat. Photonics* **2019**, *13*, 860−865.
(18) Krainer, G.; Hartmann, A.; Schlierf, M. FarFRET: Extending the Range in Single-Molecule FRET Experiments beyond 10 nm. *Nano Lett.* **2015**, *15*, 5826−5829.
(19) Maliwal, B. P.; Raut, S.; Fudala, R.; D'Auria, S.; Marzullo, V. M.; Luini, A.; Gryczynski, I.; Gryczynski, Z. Extending Förster Resonance Energy Transfer Measurements beyond 100 Å Using Common Organic Fluorophores: Enhanced Transfer in the Presence of Multiple Acceptors. *J. Biomed. Opt.* **2012**, *17*, 011006.
(20) Fábián, Á. I.; Rente, T.; Szöllősi, J.; Mátyus, L.; Jenei, A. Strength in Numbers: Effects of Acceptor Abundance on FRET Efficiency. *ChemPhysChem* **2010**, *11*, 3713−3721.
(21) Purcell, E. M. Spontaneous Emission Probabilities at Radio Frequencies. *Phys. Rev.* **1946**, *69*, 681.
(22) Drexhage, K. H. Influence of a Dielectric Interface on Fluorescence Decay Time. *J. Lumin.* **1970**, *1*−*2*, 693−701.
(23) Andrew, P.; Barnes, W. L. Förster Energy Transfer in an Optical Microcavity. *Science* **2000**, *290*, 785−788.
(24) Hsu, L.-Y.; Ding, W.; Schatz, G. C. Plasmon-Coupled Resonance Energy Transfer. *J. Phys. Chem. Lett.* **2017**, *8*, 2357−2367.
(25) Cortes, C. L.; Jacob, Z. Fundamental Figures of Merit for Engineering Förster Resonance Energy Transfer. *Opt. Express* **2018**, *26*, 19371−19387.
(26) Rustomji, K.; Dubois, M.; Kuhlmey, B.; de Sterke, C. M.; Enoch, S.; Abdeddaim, R.; Wenger, J. Direct Imaging of the Energy-Transfer Enhancement between Two Dipoles in a Photonic Cavity. *Phys. Rev. X* **2019**, *9*, 011041.
(27) Blum, C.; Zijlstra, N.; Lagendijk, A.; Wubs, M.; Mosk, A. P.; Subramaniam, V.; Vos, W. L. Nanophotonic Control of the Förster Resonance Energy Transfer Efficiency. *Phys. Rev. Lett.* **2012**, *109*, 203601.
(28) Wubs, M.; Vos, W. L. Förster Resonance Energy Transfer Rate in Any Dielectric Nanophotonic Medium with Weak Dispersion. *New J. Phys.* **2016**, *18*, 053037.
(29) Enderlein, J. Modification of Förster Resonance Energy Transfer Efficiency at Interfaces. *Int. J. Mol. Sci.* **2012**, *13*, 15227−15240.
(30) Weeraddana, D.; Premaratne, M.; Gunapala, S. D.; Andrews, D. L. Controlling Resonance Energy Transfer in Nanostructure Emitters by Positioning near a Mirror. *J. Chem. Phys.* **2017**, *147*, 074117.
(31) Wu, J.-S.; Lin, Y.-C.; Sheu, Y.-L.; Hsu, L.-Y. Characteristic Distance of Resonance Energy Transfer Coupled with Surface Plasmon Polaritons. *J. Phys. Chem. Lett.* **2018**, *9*, 7032−7039.
(32) Schleifenbaum, F.; Kern, A. M.; Konrad, A.; Meixner, A. J. Dynamic Control of Förster Energy Transfer in a Photonic Environment. *Phys. Chem. Chem. Phys.* **2014**, *16*, 12812−12817.
(33) Konrad, A.; Metzger, M.; Kern, A. M.; Brecht, M.; Meixner, A. J. Controlling the Dynamics of Förster Resonance Energy Transfer inside a Tunable Sub-Wavelength Fabry−Pérot-Resonator. *Nanoscale* **2015**, *7*, 10204−10209.
(34) Fore, S.; Yuen, Y.; Hesselink, L.; Huser, T. Pulsed-Interleaved Excitation FRET Measurements on Single Duplex DNA Molecules Inside C-Shaped Nanoapertures. *Nano Lett.* **2007**, *7*, 1749−1756.
(35) Ghenuche, P.; de Torres, J.; Moparthi, S. B.; Grigoriev, V.; Wenger, J. Nanophotonic Enhancement of the Förster Resonance Energy-Transfer Rate with Single Nanoapertures. *Nano Lett.* **2014**, *14*, 4707−4714.
(36) de Torres, J.; Ghenuche, P.; Moparthi, S. B.; Grigoriev, V.; Wenger, J. FRET Enhancement in Aluminum Zero-Mode Waveguides. *ChemPhysChem* **2015**, *16*, 782−788.
(37) Chen, J.; Dalal, R. V.; Petrov, A. N.; Tsai, A.; O'Leary, S. E.; Chapin, K.; Cheng, J.; Ewan, M.; Hsiung, P.-L.; Lundquist, P.; et al. High-Throughput Platform for Real-Time Monitoring of Biological Processes by Multicolor Single-Molecule Fluorescence. *Proc. Natl. Acad. Sci. U.S.A.* **2014**, *111*, 664−669.
(38) Zhao, Y.; Chen, D.; Yue, H.; Spiering, M. M.; Zhao, C.; Benkovic, S. J.; Huang, T. J. Dark-Field Illumination on Zero-Mode Waveguide/Microfluidic Hybrid Chip Reveals T4 Replisomal Protein Interactions. *Nano Lett.* **2014**, *14*, 1952−1960.
(39) Goldschen-Ohm, M. P.; White, D. S.; Klenchin, V. A.; Chanda, B.; Goldsmith, R. H. Observing Single-Molecule Dynamics at Millimolar Concentrations. *Angew. Chem.* **2017**, *129*, 2439−2442.
(40) Zambrana-Puyalto, X.; Maccaferri, N.; Ponzellini, P.; Giovannini, G.; De Angelis, F.; Garoli, D. Site-Selective Functionalization of Plasmonic Nanopores for Enhanced Fluorescence and Förster Resonance Energy Transfer. *Nanoscale Adv.* **2019**, *1*, 2454−2461.
(41) Zhang, J.; Fu, Y.; Chowdhury, M. H.; Lakowicz, J. R. Enhanced Förster Resonance Energy Transfer on Single Metal Particle. 2. Dependence on Donor−Acceptor Separation Distance, Particle Size, and Distance from Metal Surface. *J. Phys. Chem. C* **2007**, *111*, 11784−11792.
(42) Reil, F.; Hohenester, U.; Krenn, J. R.; Leitner, A. Förster-Type Resonant Energy Transfer Influenced by Metal Nanoparticles. *Nano Lett.* **2008**, *8*, 4128−4133.
(43) Lunz, M.; Gerard, V. A.; Gun'ko, Y. K.; Lesnyak, V.; Gaponik, N.; Susha, A. S.; Rogach, A. L.; Bradley, A. L. Surface Plasmon

https://dx.doi.org/10.1021/acsomega.0c00322
ACS Omega 2020, 5, 6947−6955

Enhanced Energy Transfer between Donor and Acceptor CdTe Nanocrystal Quantum Dot Monolayers. *Nano Lett.* **2011**, *11*, 3341−3345.
(44) Pustovit, V. N.; Shahbazyan, T. V. Resonance Energy Transfer near Metal Nanostructures Mediated by Surface Plasmons. *Phys. Rev. B: Condens. Matter Mater. Phys.* **2011**, *83*, 085427.
(45) Zhao, L.; Ming, T.; Shao, L.; Chen, H.; Wang, J. Plasmon-Controlled Förster Resonance Energy Transfer. *J. Phys. Chem. C* **2012**, *116*, 8287−8296.
(46) Gonzaga-Galeana, J. A.; Zurita-Sánchez, J. R. A Revisitation of the Förster Energy Transfer near a Metallic Spherical Nanoparticle: (1) Efficiency Enhancement or Reduction? (2) The Control of the Förster Radius of the Unbounded Medium. (3) The Impact of the Local Density of States. *J. Chem. Phys.* **2013**, *139*, 244302.
(47) Aissaoui, N.; Moth-Poulsen, K.; Käll, M.; Johansson, P.; Wilhelmsson, L. M.; Albinsson, B. FRET Enhancement Close to Gold Nanoparticles Positioned in DNA Origami Constructs. *Nanoscale* **2017**, *9*, 673−683.
(48) Bohlen, J.; Cuartero-González, Á.; Pibiri, E.; Ruhlandt, D.; Fernández-Domínguez, A. I.; Tinnefeld, P.; Acuna, G. P. Plasmon-Assisted Förster Resonance Energy Transfer at the Single-Molecule Level in the Moderate Quenching Regime. *Nanoscale* **2019**, *11*, 7674−7681.
(49) Faessler, V.; Hrelescu, C.; Lutich, A. A.; Osinkina, L.; Mayilo, S.; Jäckel, F.; Feldmann, J. Accelerating Fluorescence Resonance Energy Transfer with Plasmonic Nanoresonators. *Chem. Phys. Lett.* **2011**, *508*, 67−70.
(50) Ghenuche, P.; Mivelle, M.; de Torres, J.; Moparthi, S. B.; Rigneault, H.; Van Hulst, N. F.; García-Parajó, M. F.; Wenger, J. Matching Nanoantenna Field Confinement to FRET Distances Enhances Förster Energy Transfer Rates. *Nano Lett.* **2015**, *15*, 6193−6201.
(51) Bidault, S.; Devilez, A.; Ghenuche, P.; Stout, B.; Bonod, N.; Wenger, J. Competition between Förster Resonance Energy Transfer and Donor Photodynamics in Plasmonic Dimer Nanoantennas. *ACS Photonics* **2016**, *3*, 895−903.
(52) de Torres, J.; Mivelle, M.; Moparthi, S. B.; Rigneault, H.; Van Hulst, N. F.; García-Parajó, M. F.; Margeat, E.; Wenger, J. Plasmonic Nanoantennas Enable Forbidden Förster Dipole−Dipole Energy Transfer and Enhance the FRET Efficiency. *Nano Lett.* **2016**, *16*, 6222−6230.
(53) Zurita-Sánchez, J. R.; Méndez-Villanueva, J. Förster Energy Transfer in the Vicinity of Two Metallic Nanospheres (Dimer). *Plasmonics* **2018**, *13*, 873−883.
(54) Tumkur, T. U.; Kitur, J. K.; Bonner, C. E.; Poddubny, A. N.; Narimanov, E. E.; Noginov, M. A. Control of Förster Energy Transfer in the Vicinity of Metallic Surfaces and Hyperbolic Metamaterials. *Faraday Discuss.* **2015**, *178*, 395−412.
(55) Roth, D. J.; Nasir, M. E.; Ginzburg, P.; Wang, P.; Le Marois, A.; Suhling, K.; Richards, D.; Zayats, A. V. Förster Resonance Energy Transfer inside Hyperbolic Metamaterials. *ACS Photonics* **2018**, *5*, 4594−4603.
(56) Levene, M. J.; Korlach, J.; Turner, S. W.; Foquet, M.; Craighead, H. G.; Webb, W. W. Zero-Mode Waveguides for Single-Molecule Analysis at High Concentrations. *Science* **2003**, *299*, 682−686.
(57) Zhu, P.; Craighead, H. G. Zero-Mode Waveguides for Single-Molecule Analysis. *Annu. Rev. Biophys.* **2012**, *41*, 269−293.
(58) Baibakov, M.; Patra, S.; Claude, J.-B.; Moreau, A.; Lumeau, J.; Wenger, J. Extending Single-Molecule Förster Resonance Energy Transfer (FRET) Range beyond 10 Nanometers in Zero-Mode Waveguides. *ACS Nano* **2019**, *13*, 8469−8480.
(59) Zanetti-Domingues, L. C.; Tynan, C. J.; Rolfe, D. J.; Clarke, D. T.; Martin-Fernandez, M. Hydrophobic Fluorescent Probes Introduce Artifacts into Single Molecule Tracking Experiments Due to Non-Specific Binding. *PLoS One* **2013**, *8*, No. e74200.
(60) Hughes, L. D.; Rawle, R. J.; Boxer, S. G. Choose Your Label Wisely: Water-Soluble Fluorophores Often Interact with Lipid Bilayers. *PLoS One* **2014**, *9*, No. e87649.
(61) Hua, B.; Han, K. Y.; Zhou, R.; Kim, H.; Shi, X.; Abeysirigunawardena, S. C.; Jain, A.; Singh, D.; Aggarwal, V.; Woodson, S. A.; Ha, T. An Improved Surface Passivation Method for Single-Molecule Studies. *Nat. Methods* **2014**, *11*, 1233−1236.
(62) Patra, S.; Baibakov, M.; Claude, J.-B.; Wenger, J. Surface Passivation of Zero-Mode Waveguide Nanostructures: Benchmarking Protocols and Fluorescent Labels. **2020**, arXiv:2001.04718 [physis].
(63) Holzmeister, P.; Acuna, G. P.; Grohmann, D.; Tinnefeld, P. Breaking the Concentration Limit of Optical Single-Molecule Detection. *Chem. Soc. Rev.* **2014**, *43*, 1014−1028.
(64) Punj, D.; Ghenuche, P.; Moparthi, S. B.; de Torres, J.; Grigoriev, V.; Rigneault, H.; Wenger, J. Plasmonic Antennas and Zero-Mode Waveguides to Enhance Single Molecule Fluorescence Detection and Fluorescence Correlation Spectroscopy toward Physiological Concentrations. *Wiley Interdiscip. Rev.: Nanomed. Nanobiotechnol.* **2014**, *6*, 268−282.
(65) Müller, B. K.; Zaychikov, E.; Bräuchle, C.; Lamb, D. C. Pulsed Interleaved Excitation. *Biophys. J.* **2005**, *89*, 3508−3522.
(66) Rüttinger, S.; Macdonald, R.; Krämer, B.; Koberling, F.; Roos, M.; Hildt, E. Accurate Single-Pair Förster Resonant Energy Transfer through Combination of Pulsed Interleaved Excitation, Time Correlated Single-Photon Counting, and Fluorescence Correlation Spectroscopy. *J. Biomed. Opt.* **2006**, *11*, 024012.
(67) Wenger, J.; Gérard, D.; Aouani, H.; Rigneault, H.; Lowder, B.; Blair, S.; Devaux, E.; Ebbesen, T. W. Nanoaperture-Enhanced Signal-to-Noise Ratio in Fluorescence Correlation Spectroscopy. *Anal. Chem.* **2009**, *81*, 834−839.
(68) Flauraud, V.; Regmi, R.; Winkler, P. M.; Alexander, D. T. L.; Rigneault, H.; van Hulst, N. F.; García-Parajo, M. F.; Wenger, J.; Brugger, J. In-Plane Plasmonic Antenna Arrays with Surface Nanogaps for Giant Fluorescence Enhancement. *Nano Lett.* **2017**, *17*, 1703−1710.
(69) Bouchet, D.; Cao, D.; Carminati, R.; De Wilde, Y.; Krachmalnicoff, V. Long-Range Plasmon-Assisted Energy Transfer between Fluorescent Emitters. *Phys. Rev. Lett.* **2016**, *116*, 037401.
(70) de Torres, J.; Ferrand, P.; Colas des Francs, G.; Wenger, J. Coupling Emitters and Silver Nanowires to Achieve Long-Range Plasmon-Mediated Fluorescence Energy Transfer. *ACS Nano* **2016**, *10*, 3968−3976.
(71) Aeschlimann, M.; Brixner, T.; Cinchetti, M.; Frisch, B.; Hecht, B.; Hensen, M.; Huber, B.; Kramer, C.; Krauss, E.; Loeber, T. H.; Pfeiffer, W.; Piecuch, M.; Thielen, P. Cavity-Assisted Ultrafast Long-Range Periodic Energy Transfer between Plasmonic Nanoantennas. *Light: Sci. Appl.* **2017**, *6*, No. e17111.
(72) de Roque, P. M.; van Hulst, N. F.; Sapienza, R. Nanophotonic Boost of Intermolecular Energy Transfer. *New J. Phys.* **2015**, *17*, 113052.
(73) McPeak, K. M.; Jayanti, S. V.; Kress, S. J. P.; Meyer, S.; Iotti, S.; Rossinelli, A.; Norris, D. J. Plasmonic Films Can Easily Be Better: Rules and Recipes. *ACS Photonics* **2015**, *2*, 326−333.
(74) Kudryavtsev, V.; Sikor, M.; Kalinin, S.; Mokranjac, D.; Seidel, C. A. M.; Lamb, D. C. Combining MFD and PIE for Accurate Single-Pair Förster Resonance Energy Transfer Measurements. *ChemPhysChem* **2012**, *13*, 1060−1078.

https://dx.doi.org/10.1021/acsomega.0c00322
ACS Omega 2020, 5, 6947−6955